30. J. B. Jupiter, *J. Bone J. Surg. Am. Vol.* **73**, 461 (1991).
31. J. J. Dias, C. C. Wray, J. M. Jones, *Injury* **18**, 304 (1987); C. Pool, *J. Bone Jt. Surg. Br. Vol.* **55**, 540 (1973); A. Schmalholz, *Clin. Orthop. Relat. Res.* **254**, 236 (1990).
32. E. Fess, *Clinical Assessment Recommendations* (American Society of Hand Therapists, Chicago, 1992), pp. 41–45.
33. In a pilot wrist fracture clinical study conducted at Lund University Hospital, Lund, Sweden, which treated patients who had already failed reduction under conventional casting, patients had their fractures re-reduced and the new biomaterial was introduced. The patients were then re-casted; the cast was left on for only 2 weeks, then removed, and the patients were allowed to begin physical therapy. These patients achieved functional recovery very early, suggesting that extended casting (6 weeks) or immobilization through external fixation (8 to 10 weeks) could be shortened significantly or eliminated completely when the new biomaterial has been implanted in the fracture site.
34. We thank the reviewers for useful comments and the assistance of the Brookhaven National Laboratory (K. D'Amico), the Letterman Army Institute of Research (J. Baker, W. Rodkey, T. Bozo, D. Fredericks, W. Bergman, and L. McKinney), the University of Michigan Orthopaedic Research Laboratory and the Cleveland Clinic Foundation (E. Frankenburg, T. Bauer, J. Baker, and K. Sweet), Massachusetts General Hospital (L. Goodman, S. Simpson, S. Winters, S. Sigmund, C. Pappas, and C. Lowe), and Norian Corporation (R. Sakai, who prepared all aspects of the manuscript, K. Alcorn, and B. Barr) whose participation made this report possible.

7 September 1994; accepted 18 January 1995

Spontaneous Magnetic Ordering in the Fullerene Charge-Transfer Salt (TDAE)C_{60}

A. Lappas, K. Prassides,* K. Vavekis, D. Arcon, R. Blinc, P. Cevc, A. Amato, R. Feyerherm, F. N. Gygax, A. Schenck

The zero-field muon spin relaxation technique has been used in the direct observation of spontaneous magnetic order below a Curie temperature (T_C) of ~16.1 kelvin in the fullerene charge-transfer salt (tetrakisdimethylaminoethylene)C_{60} [(TDAE)C_{60}]. Coherent ordering of the electronic magnetic moments leads to a local field of 68(1) gauss at the muon site at 3.2 kelvin (parentheses indicate the error in the last digit). Substantial spatially inhomogeneous effects are manifested in the distribution of the local fields, whose width amounts to 48(2) gauss at the same temperature. The temperature evolution of the internal magnetic field below the freezing temperature mirrors that of the saturation magnetization, closely following the behavior expected for collective spin wave (magnon) excitations. The transition to a ferromagnetic state with a T_C higher than that of any other organic material is now authenticated.

Intercalation of solid C_{60} with electron donors, such as the alkali metals, can lead to metallic compositions of stoichiometry A_3C_{60} that become superconducting (*1*) at critical temperatures as high as 33 K, surpassed only by the superconducting cuprates with high superconducting transition temperatures. Reactions of C_{60} with strong organic donors, such as tetrakisdimethylaminoethylene, $C_2N_4(CH_3)_8$ (Fig. 1), also result in materials with interesting properties. The charge-transfer salt with stoichiometry (TDAE)C_{60} develops a large magnetic susceptibility below ~16.1 K, consistent with a transition to a ferromagnetic state (*2*). The lack of any observed remanent magnetization or hysteresis was interpreted in terms of "soft" ferromagnetism (*3*) in a highly anisotropic solid, as necessitated by a crystal structure in which there were relatively short (~9.96 Å) intermolecular contacts along the *c* axis (*4*). The ferromagnetic state was also found to be highly sensitive to applied pressure, with both the magnetic moment and the transition temperature decreasing rapidly (*3*, *5*). The conductivity at room temperature is of the order of $\sim 10^{-4}$ ohm^{-1} cm^{-1} and shows a nonmetallic temperature dependence (*6*). Despite numerous efforts with various experimental techniques, such as magnetization (*7*), electron spin resonance (ESR) (*7–10*), and nuclear magnetic resonance (NMR) (*9*, *11*) measurements, the origin and true nature of the low-temperature magnetic phase has remained the subject of controversy, encompassing the possibilities of field-induced "weak" ferromagnetism, "itinerant" ferromagnetism, "spin glass"–like ordering, and "superparamagnetic"-type ordering. However, as yet the most fundamental parameter of a ferromagnet, the spontaneous magnetization in zero applied field, has remained uninvestigated.

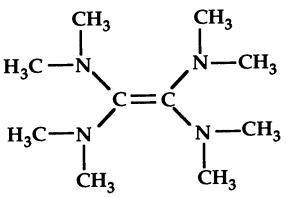

Fig. 1. The TDAE molecule.

Here, we address the problem of the existence of nonzero internal local fields in the low-temperature phase of (TDAE)C_{60}. We investigated this problem by using 100% spin-polarized positive muons (μ^+) in the absence of external fields. These muons are implanted into the solid sample and, after they come to rest at an interstitial site, they act as highly sensitive microscopic local magnetic probes. In the presence of local magnetic fields ($\langle B_\mu \rangle$), they will precess with a frequency given by

$$\nu_\mu = (\gamma_\mu/2\pi)\langle B_\mu \rangle \quad (1)$$

where $\gamma_\mu/2\pi = 13.55$ kHz G^{-1}. In the absence of an applied external field, the appearance of precession signals the onset of an ordering (ferromagnetic or antiferromagnetic) transition. Moreover, application of a magnetic field parallel to the initial muon spin polarization [longitudinal field (LF)] allows the decoupling of the μ^+ spin from the static internal fields. Muon spin relaxation (μ^+SR) spectroscopy has proven extremely powerful in cases of small-moment magnetism and in all instances where magnetic order is of a random, very short range, spatially inhomogeneous or incommensurate nature (*12*). In (TDAE)C_{60}, we observed a heavily damped oscillating signal, which provides unambiguous proof of the existence of long-range magnetic order below ~16.1 K. The strong relaxation found in zero field (ZF) is the signature of spatial disorder and inhomogeneity effects. In addition, we found that the precession frequency varies with temperature on approaching the Curie temperature (T_C) in a different manner from that expected on the basis of the mean-field treatment of a three-dimensional Heisenberg exchange model. It appears that magnon excitations dominate the magnetic behavior, even at temperatures close to T_C, thus providing an explanation of the observed properties, such as the "soft" magnetic behavior, the small saturated moment per molecule [0.33 Bohr magneton (μ_B) at 5 K], the pressure sensitivity of the magnetic properties, and the spatial disorder.

We collected ZF and LF (10 to 1000 G) μ^+SR data on (TDAE)C_{60} (*13*) at the Paul Scherrer Institute (PSI), Villigen, Switzerland, with the general purpose spectrometer, using low-energy (surface) muons on the μ^+SR-dedicated πM3 beamline on the PSI 600-MeV proton accelerator. The 120-mg powder sample was sealed under Ar in an Ag sample holder equipped with In seals

A. Lappas, K. Prassides, K. Vavekis, School of Chemistry and Molecular Sciences, University of Sussex, Brighton BN1 9QJ, U.K.
D. Arcon, R. Blinc, P. Cevc, J. Stefan Institute, University of Ljubljana, 61111 Ljubljana, Slovenia.
A. Amato, R. Feyerherm, F. N. Gygax, A. Schenck, Institute for Particle Physics, Swiss Federal Institute of Technology (ETH) Zürich, CH-5232, Paul Scherrer Institute, Villigen, Switzerland.
*To whom correspondence should be addressed.

and Mylar windows and placed inside a continuous-flow He cryostat, allowing measurements down to 3.2 K. The sample was cooled slowly from room temperature over a period of 2 hours, and measurements were performed both on heating and on cooling. Transverse-field (TF) data were also collected at 300 K at an applied field of 5 kG to search for radical formation and at 50 K at an applied field of 20 G for calibration purposes.

Signals from paramagnetic muonium ($Mu \equiv \mu^+e^-$) centers with an isotropic hyperfine constant, A_{hf} = 324.4(1) MHz, coexisted with the diamagnetic μ^+ signal in the room-temperature 5-kG TF data. They correspond to a volume fraction of the sample of ~10% and are assigned to the formation of MuC_{60} radicals (*14*), consistent with the presence of the unreacted C_{60} identified by x-ray diffraction (XRD). No other radical (for example, muonated TDAE) species was evident. In Fig. 2, we show the ZF time-dependent μ^+SR spectra of (TDAE)-C_{60} at various temperatures between 3.2 and 16.8 K. No oscillating signal was seen at 16.8 K and above. The μ^+SR spectra in the high-temperature range of the present experiments (16.8 to 50 K) are characteristic of the presence of weak static nuclear dipole moments, which result in a small depolarization rate, σ = 0.151(4) μs^{-1}. This muon relaxation arises from the hydrogen nuclear moments that appear frozen into a disordered spin configuration, producing an essentially temperature-independent distribution of local fields with a width, $\langle \Delta B^2 \rangle^{1/2}$, of 1.77(5) G and implies a distance of the μ^+ from the nearest H atoms of ~2 Å. We also identified the presence of a minority (~10% by volume) short-lived, essentially temperature-independent signal whose relaxation is attributed to the triplet component of the muonated fullerene radicals, associated with the unreacted C_{60}. This masks any additional relaxation of the μ^+ polarization that may originate from fluctuating electronic moments and precludes us from obtaining any information on the critical slowing down of the electronic spin dynamics within the paramagnetic domains down to 16.8 K.

Below 16.8 K (Fig. 2), there is a short-lived signal whose depolarization gradually increases with decreasing temperature. We used several different relaxation functions in the fitting procedure in an effort to reveal the correct microscopic mechanism responsible for the depolarization of the muon spin. The Uemura spin glass function (*15*) could not fit the data satisfactorily over the whole temperature range (*16*). The time-dependent asymmetry shows a rapid decay at time $t < 0.1$ μs, a minimum between 0.1 and 0.2 μs, and a recovery at $t > 0.2$ μs. At long times ($t \gg 1$ μs), the asymmetry continues to relax at an increasing rate with increasing temperature.

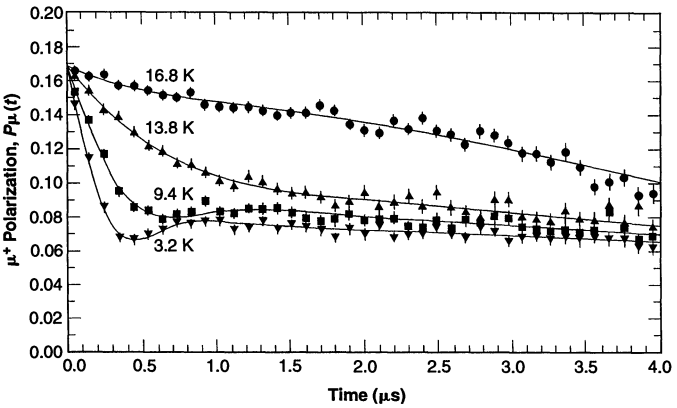

Fig. 2. Evolution of the zero-field μ^+ polarization $P_\mu(t)$ at various temperatures for $(TDAE)C_{60}$. The solid line through the 16.8 K data is a fit to the sum of a static Kubo-Toyabe function (*17*), reflecting the presence of weak static nuclear dipole moments, and an exponentially relaxing function, reflecting the presence of paramagnetic muonium centers, associated with the unreacted C_{60}. The solid lines through the data at all other temperatures are fits to the two-component function of Eq. 2, which includes one short-lived oscillating and one long-lived nonoscillating component.

These characteristics are also similar to the features of the dynamic Kubo-Toyabe relaxation function (*17*), appropriate for a Gaussian distribution of fluctuating random fields of width Δ whose fluctuation rate, ν, decreases with decreasing temperature. Even though this function can provide an appealing description of the low-temperature magnetic phase of $(TDAE)C_{60}$, consistent with observations of earlier ESR and NMR measurements (*7–11*), it is inappropriate (*18*) on the evidence of the complementary LF μ^+SR data, collected at temperatures between 3.2 and 35 K. The effect of applied LFs is to allow the depolarization due to dynamic or fluctuating moments to be decoupled from that due to static components. Figure 3 shows the 1-kG LF data at 3.2 and 13.8 K. There has been a complete recovery of the asymmetry at long times with no evidence for any remaining dynamic fields. In contrast, the dynamic Kubo-Toyabe function requires in the present case fluctuating random fields whose fluctuation rate increases gradually from ~0.6 μs^{-1} at 3.2 K ($\nu/\Delta < 1$) to ~13 μs^{-1} at 13.8 K ($\nu/\Delta > 1$). This necessitates an alternative interpretation of the experimental data.

We thus explored the fitting of the data with a strongly damped oscillating polarization signal superimposed on a slowly relaxing component of the form

$$P_\mu(t) = A_1 e^{-\lambda_1 t}\cos(2\pi\nu_\mu t + \phi) + A_2 e^{-\lambda_2 t} \quad (2)$$

where A_1 and A_2 are amplitudes reflecting the fractions of the muons contributing to the two components, $\nu_\mu = \omega_\mu/2\pi$ is the μ^+ Larmor precession frequency and ϕ is its phase, and λ_1 and λ_2 are exponential relaxation rates associated with the two components. The physical origin of Eq. 2 lies with the fact that, on average, for a completely random distribution of the directions of the internal field in a powder sample, one-third of all muons will experience an internal field along their initial spin direction and consequently they will not precess, giving rise to the second term on the right in Eq. 2; λ_2 thus represents relaxation due to fluctuating field components perpendicular to the μ^+ spin. In contrast, λ_1 reflects relaxation due to both dynamic- and static-field inhomogeneities. In addition, the ideal ratio of the asymmetries of the two components is $A_2/A_1 = 0.5$.

The model function of Eq. 2 led to immediate convergence, while the total ($A_1 + A_2$) zero-time asymmetry was constrained to the value obtained in the weak TF run at 50 K. The observation of ν_μ in zero external field indicates the onset of magnetic order, where the spontaneous magnetization is proportional to ν_μ. The frequency ν_μ is 0.92(2) MHz at the lowest measured temperature of 3.2 K and corresponds to a static local field at the muon site of $\langle B_\mu \rangle$ = 68(1) G. This is about half the frequency observed in the β phase of the organic radical ferromagnet (*19*) *p*-nitrophenyl nitronyl nitroxide (T_C = 0.67 K). In addition, the depolarization rate λ_1 reaches a value of 4.1(2) μs^{-1} at 3.2 K, implying a distribution of local fields with a width $\langle \Delta B^2 \rangle^{1/2}$ = 48(2) G—only smaller than $\langle B_\mu \rangle$ by a factor of 1.4—and placing the μ^+ ~4.3 Å from the fullerene molecules. The muons thus experience a local field with large spatial inhomogeneities that may be due to a number of physical factors, including orientational disorder effects of the fullerene molecules invariably present both in pristine fullerenes and in their intercalated derivatives (*20*), spin glass–type effects that could coexist with the long-range magnetic order (*11*, *21*), or incommensurate order between the crystallographic and magnetic structures [compare the incommensurate organic spin-density-wave systems, $(TMTSF)_2X$ (*22*), where TMTSF is tetramethyltetraselenaful-

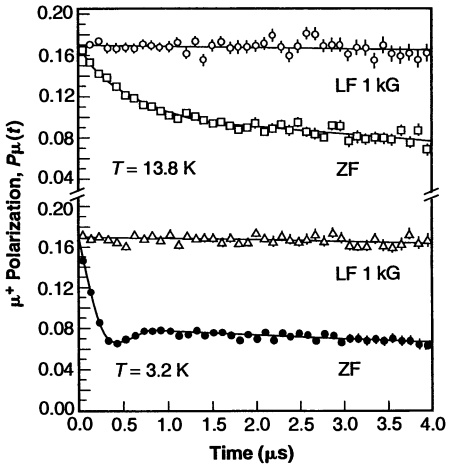

Fig. 3. Zero-field (ZF) and longitudinal-field (LF, 1 kG) μ^+SR time spectra of $(TDAE)C_{60}$ at 3.2 and 13.8 K.

valene and X is PF_6, NO_3, or ClO_4].

The unconventional form of magnetism in $(TDAE)C_{60}$ is also apparent in Fig. 4A, which shows the temperature dependence of the spontaneous precession frequency extracted from the fits to Eq. 2. The variation of $\nu_\mu(T)$ with temperature is fitted very well over the whole temperature range of the present experiment by Bloch's $T^{3/2}$ law,

$$\nu_\mu(T) = \nu(0)(1 - AT^{3/2}) \qquad (3)$$

with $\nu(0) = 1.01(2)$ MHz and $A = 1.55(4) \times 10^{-2}$ $K^{-3/2}$ [leading to an ordering temperature, $T_C = 16.1(3)$ K]. This behavior deviates from the conventional behavior of a three-dimensional Heisenberg spin system, which is characterized by a critical exponent $\beta = 0.367$ close to T_C and a magnon-like behavior at low temperatures.

One explanation for the observed behavior is that in $(TDAE)C_{60}$ the presence of spin wave excitations (magnons) is not only dominant at very low temperatures but survives close to the ordering temperature. The transition to the ferromagnetically ordered state should then involve consideration of extended exchange interactions beyond nearest neighbors and should perhaps be understood as the Bose condensation of the magnon excitations. Alternatively, the magnon-like behavior may reflect a more complicated physical picture of the system, where the intrinsic orientational disorder associated with the fullerene molecules gives rise to a broad distribution of exchange constants (and ordering temperatures). Combining our results with magnetization $M(5\text{ K}) = 0.33$ μ_B per molecule (4) obtained by magnetization measurements, we find $M(0\text{ K}) \approx 0.4$ μ_B per molecule, very different from 1 μ_B per molecule.

In Fig. 4A, we have also included the magnetization data (at 100 G) from (2) that closely mimic the temperature evolution of

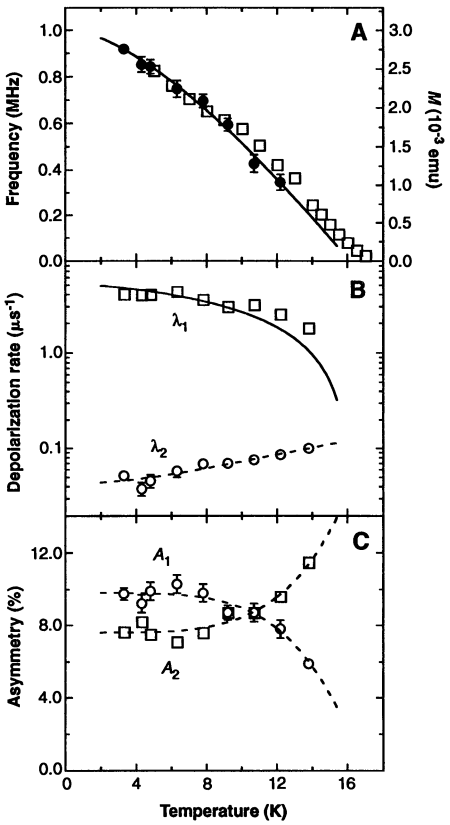

Fig. 4. Temperature dependence of (**A**) the muon precession frequency, ν_μ (solid circles), and the magnetization at 100 G, M (open squares), from (2) (the solid line is a fit to Bloch's $T^{3/2}$ law) (emu, electromagnetic unit); (**B**) the depolarization rates of the oscillating, λ_1 (open squares), and nonoscillating, λ_2 (open circles), components; the solid line through the λ_1 points is the line resulting from a fit of Bloch's $T^{3/2}$ law to the frequency data, and the broken line through the λ_2 points is a guide to the eye; (**C**) the asymmetries A_1 (open squares) and A_2 (open circles) of the two components; the broken lines represent guides to the eye.

$\nu_\mu(T)$. This can be understood if we recall that for a ferromagnet the effective magnetic field at the muon site in the absence of an external field is made up by contributions from dipolar and transferred hyperfine (B_{hyp}) fields and the Lorentz field, $B_L = (4/3)\pi M_s$, where M_s is the saturation magnetization. The temperature evolution of $\nu_\mu(T)$ primarily reflects that of B_{hyp} and B_L. The depolarization rate, λ_1 (Fig. 4B), also displays a temperature dependence similar to that of $\nu_\mu(T)$. The depolarization rate, λ_2, of the nonoscillating component (the second term on the right in Eq. 2) (Fig. 4B) normally arises from fluctuations of the local field components perpendicular to the μ^+ spin polarization. However, as the LF data reveal purely static behavior, the observed relaxation should be affected by the presence of paramagnetic muonium centers in the unreacted C_{60} part of the sample and of nuclear dipole fields.

Finally, as the temperature is lowered (Fig. 4C), the volume fraction of the nonoscillating component becomes smaller, while the first term on the right in Eq. 2, which gives rise to the oscillating signal, begins to dominate at lower temperatures as the volume fraction of the magnetically ordered domains grows at the expense of the paramagnetic ones. The ratio of the asymmetries (A_2/A_1) of the two components approaches a value of ~0.7 at low temperatures, larger than the value of 0.5 expected for a polycrystalline sample in which practically no paramagnetic contributions are detected by the μ^+ below T_C. The discrepancy presumably arises because the nonoscillating signal includes contributions from the minority C_{60} phase; if its volume fraction is subtracted out, the ratio of the asymmetries in the $(TDAE)C_{60}$ part of the sample is close to 0.5, as expected from a complete random distribution of directions in a polycrystalline sample.

Additional μ^+SR experiments at lower temperatures and as a function of field are needed to obtain further insights about the magnetism in this material. Neutron scattering experiments should also provide valuable information.

REFERENCES AND NOTES

1. A. F. Hebard *et al.*, *Nature* **350**, 600 (1991); K. Holczer *et al.*, *Science* **252**, 1154 (1991); K. Tanigaki *et al.*, *Nature* **352**, 222 (1991).
2. P.-M. Allemand *et al.*, *Science* **253**, 301 (1991).
3. F. Wudl and J. D. Thompson, *J. Phys. Chem. Solids* **53**, 1449 (1992).
4. P. W. Stephens *et al.*, *Nature* **355**, 331 (1992).
5. G. Sparn *et al.*, *Solid State Commun.* **82**, 779 (1992).
6. A. Schilder *et al.*, *Phys. Rev. Lett.* **73**, 1299 (1994).
7. K. Tanaka *et al.*, *Phys. Rev. B* **47**, 7554 (1993).
8. P. Cevc *et al.*, *Europhys. Lett.* **26**, 707 (1994); *Solid State Commun.* **90**, 543 (1994).
9. P. Venturini *et al.*, *Int. J. Mod. Phys. B* **23**, 3947 (1992).
10. R. Seshadri *et al.*, *Solid State Commun.* **85**, 971 (1993).
11. R. Blinc *et al.*, *ibid.* **89**, 487 (1994).
12. A. Schenck, in *Frontiers in Solid State Science*, L. C. Gupta and M. S. Multani, Eds. (World Scientific, Singapore, 1993), vol. 2, pp. 269–361.
13. The $(TDAE)C_{60}$ sample was synthesized by direct reaction between C_{60} and excess TDAE in an Ar atmosphere. After the excess TDAE had been removed by filtering, the $(TDAE)C_{60}$ precipitate was repeatedly washed with hexane and dried under vacuum. The present sample was thoroughly characterized by XRD, ESR, and NMR measurements. Powder XRD measurements on samples sealed in thin-walled capillaries gave profiles identical to those previously reported (*4*), consisting of strong, sharp peaks from monoclinic $(TDAE)C_{60}$, together with additional peaks from coexisting face-centered-cubic C_{60}. It has not been possible to obtain samples free of unreacted C_{60}, in agreement with earlier reports (*2, 4*). The magnetic transition at 16.1 K was also confirmed in the present sample by ESR measurements.
14. E. J. Ansaldo, C. Niedermayer, C. E. Stronach, *Nature* **353**, 129 (1991).
15. Y. J. Uemura *et al.*, *Phys. Rev. B* **31**, 546 (1985).
16. Earlier μ^+SR measurements on $(TDAE)C_{60}$ [M. Riccò, L. Cristofolini, R. De Renzi, G. Ruani, in *Recent Advances in the Chemistry and Physics of Fullerenes and Related Materials*, K. M. Kadish and R. S. Ruoff, Eds. (Electrochemical Society, Penning-

ton, NJ, 1994), pp. 1187–1202] at the pulsed muon facility at the Rutherford Appleton Laboratory have been interpreted in terms of a spin glass–like model (random static moments). However, these data have the disadvantage that the rapid initial decay of the μ^+ spin depolarization was not observed, thus making reliable inferences about the nature of the magnetic phase problematic.
17. R. Kubo and T. Toyabe, in *Magnetic Resonance and Relaxation*, R. Blinc, Ed. (North-Holland, Amsterdam, 1967), pp. 810–823; R. S. Hayano *et al.*, *Phys. Rev. B* **20**, 850 (1979).
18. Another feature of the experimental data that mitigates against the use of a Kubo-Toyabe (static or dynamic) function is that the ZF asymmetry never recovers in the vicinity of ~2 μs to a value approximately equal to one-third of the initial asymmetry at time zero.
19. J. P. Le *et al.*, *Chem. Phys. Lett.* **206**, 405 (1993).
20. K. Prassides, in *Recent Advances in the Chemistry and Physics of Fullerenes and Related Materials*, K. M. Kadish and R. S. Ruoff, Eds. (Electrochemical Society, Pennington, NJ, 1994), pp. 477–497.
21. D. Sherrington and S. Kirkpatrick, *Phys. Rev. Lett.* **35**, 1792 (1975); M. Gabay and G. Toulouse, *ibid.* **47**, 201 (1981).
22. J. P. Le *et al.*, *Europhys. Lett.* **15**, 547 (1991); *Phys. Rev. B* **48**, 7284 (1993).
23. Supported by the Engineering and Physical Sciences Research Council (United Kingdom). We thank the Paul Scherrer Institute for provision of beam time, D. Herlach for technical help with the experiments, and L. Cristofolini for useful discussions.

27 October 1994; accepted 26 January 1995

Kinetics of Conversion of Air Bubbles to Air Hydrate Crystals in Antarctic Ice

P. B. Price

The depth dependence of bubble concentration at pressures above the transition to the air hydrate phase and the optical scattering length due to bubbles in deep ice at the South Pole are modeled with diffusion-growth data from the laboratory, taking into account the dependence of age and temperature on depth in the ice. The model fits the available data on bubbles in cores from Vostok and Byrd and on scattering length in deep ice at the South Pole. It explains why bubbles and air hydrate crystals coexist in deep ice over a range of depths as great as 800 meters and predicts that at depths below ~1400 meters the AMANDA neutrino observatory at the South Pole will operate unimpaired by light scattering from bubbles.

Ancient air is known to be trapped in polar ice at depths below the layer of firn (that is, porous) ice. Early investigations showed that the air was trapped in bubbles that decreased in size and concentration with increasing depth. To account for the disappearance of bubbles at great depth, Miller (*1*) predicted that the bubbles would convert into a clathrate hydrate phase at depths corresponding to a pressure greater than that for formation of that phase. He showed that the phase consists of a cubic crystal structure in which O_2 and N_2 molecules from air are trapped in clathrate cages. If O_2 and N_2 occur in atmospheric proportions, the crystals are usually referred to as air hydrate crystals. The hatched region in Fig. 1 shows Miller's calculated curves for the temperature dependence of the formation pressure for nitrogen hydrate and for air hydrate, displayed on a scale in which pressure has been converted to depth in ice. The curves labeled for ice at four Antarctic sites and two Greenland sites show temperature as a function of depth (*2*–*6*). Koci (*6*) modeled the temperature versus depth at South Pole, using the known surface temperature of −55°C and fixing the temperature at bedrock at the pressure melting temperature. In situ measurements (*7*) by AMANDA at depths from 800 to 1000 m gave temperatures that agreed with Koci's model to within 0.3°C.

Over a wide range of depths, bubbles and air hydrate crystals are seen to coexist (Fig. 1). For Vostok and Byrd cores, quantitative measurements have been made of concentrations and sizes of bubbles (*8*, *9*) and air hydrate crystals (*10*, *11*). For Dome C, Dye 3, and Camp Century cores, Shoji and Langway (*12*, *13*) reported only qualitative data on air hydrates. For the South Pole, no deep core has yet been obtained.

This paper poses solutions to several puzzles: Why do bubbles and air hydrate crystals coexist over a range of depths as great as 800 m? In particular, why does it take so long for bubbles to disappear at pressures at which they are unstable against the phase transition? Why do the depths of disappearance of bubbles in various cores not show some systematic dependence on depth or temperature? Based on the measurements on bubbles at Vostok and Byrd, can we predict the concentration of bubbles as a function of depth in ice at the South Pole? The last question is of great importance to the AMANDA project (*14*, *15*), which involves implanting long strings of large photomultiplier tubes at great depths in South Pole ice in order to detect Cherenkov light from muons produced in high-energy neutrino interactions. Only if the array is located in bubble-free ice can the direction of a muon be precisely determined by measurement of the arrival times of the Cherenkov wave front at each of the phototubes.

Several studies of the transformation of air bubbles into air hydrate crystals have been done in pressure cells on time scales up to a few days at temperatures from −20° to −2°C and at pressures up to ~8 MPa. Using a high-pressure cell on a microscope stage, Uchida *et al.* (*16*) studied the growth of air hydrate crystals on the walls of bubbles in a sample of Vostok core taken from a depth of 1514 m. Because of relaxation after recovery of the core, the original air hydrate crystals had converted back into bubbles before Uchida *et al.* started the experiment. They observed the growth rate of air hydrate crystals as a function of supersaturation, dP/P_e, at temperatures just below the melting point of ice (where P is the hydrostatic pressure on the system and P_e is the equilibrium pressure at the phase boundary). They found that for $dP/P_e > 0.35$, the crystals grew as spherical shells coating the bubble walls.

Continuing this line of research, Uchida *et al.* (*17*) showed that two activation energies were involved. Before a thin shell of air hydrate crystal had completely coated

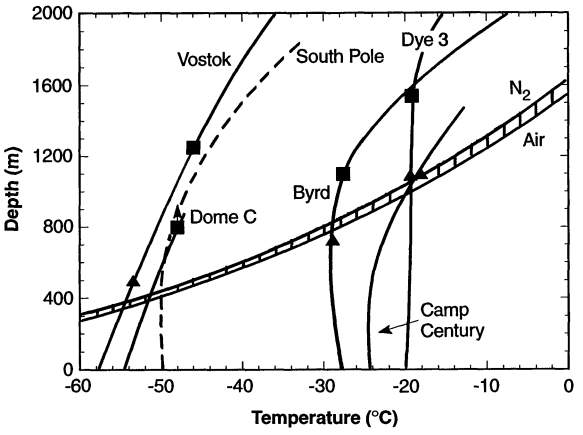

Fig. 1. Temperature as a function of depth in ice, compared with equilibrium pressures (converted to depths) for coexistence of the (bubble + ice) phase and the air hydrate phase. Upper boundary of the hatched region is for nitrogen-clathrate-hydrate; lower boundary is for air-clathrate-hydrate. Squares indicate the depths in cores below which air bubbles are not observed. The arrow on the square for Dome C indicates that air hydrate crystals were present to the bottom of the core. Triangles indicate the depths below which air hydrate crystals are observed.

Physics Department, University of California, Berkeley, CA 94720, USA.